JBMR Plus, 2025, **9**, ziae121
https://doi.org/10.1093/jbmrpl/ziae121
Advance access publication: September 17, 2024
Research Article

Differential microRNA expression patterns between TallyHo/JngJ mice and non-diabetic Swiss Webster Random/Jackson mice

David Carro Vázquez[1], Lejla Emini[2], Martina Rauner[2], Christine Hofbauer[2], Susanna Skalicky[1], Alisia Wagner[1], Johannes Grillari[3,4,5], Andreas B. Diendorfer[1], Lorenz C. Hofbauer[2], Matthias Hackl[1,5,*]

[1]TAmiRNA GmbH, Department of Research and Development, 1110 Vienna, Austria
[2]Department of Medicine III and Center for Healthy Aging, Technische Universität Dresden Medical Center, 01307 Dresden, Germany
[3]Ludwig Boltzmann Institute for Traumatology, The Research Center in Cooperation with AUVA, 1200 Vienna, Austria
[4]Department of Biotechnology, Institute of Molecular Biotechnology, University of Natural Resources and Life Sciences, 1190 Vienna, Austria
[5]Austrian Cluster for Tissue Regeneration, 1200 Vienna, Austria

*Corresponding author: Matthias Hackl, TAmiRNA GmbH, Leberstraße 20, 1110 Vienna, Austria (matthias.hackl@tamirna.com).

Abstract

Type 2 diabetes mellitus (T2DM) increases the susceptibility of bone fragility. The underlying mechanisms have, however, remained largely unknown. MicroRNAs (miRNAs) are short single-stranded non-coding RNA molecules with utility as biomarkers due to their easy accessibility and stability in bodily fluids. Here, we aimed to use an unbiased approach to identify miRNAs dysregulated in a polygenic mouse model of T2DM. Genome-wide analysis of miRNAs in serum, BM, and bone from the polygenic TallyHo/JngJ (TH) mice, which recapitulate T2DM in humans, was performed. This analysis was compared to the recommended control Swiss Webster Random/Jackson (SWR/J) and a strain-matched non-diabetic control (TH-ND). When comparing TH mice with TH-ND using an adjusted *p*-value false discovery rate (FDR) cut-off of 0.2 to identify differentially expressed miRNAs, mmu-miR-466i-5p and mmu-miR-1195 were found to be up-regulated in both serum and in BM. Dysregulated miRNAs were not found in bone tissue. When comparing TH-ND mice with SWR/J using the same FDR cut-off, mmu-miR-351-5p, and mmu-miR-322-3p were upregulated in both BM and serum, while mmu-miR-449a-5p and mmu-miR-6240 were downregulated in BM and serum. Dysregulated miRNAs in BM or cortical bone compared to serum between TH-ND mice and SWR/J were investigated for their cell-type enrichment to identify putative donor cells and their gene target networks. Gene target network analysis revealed genes involved in diabetes-related signaling pathways as well as in diabetic bone disease. Cell-type enrichment analysis identified hsa-miR-449a enriched in immune cells, hsa-miR-592 in hepatocytes and endothelial cells, while hsa-miR-424-3p, hsa-miR-1-3p, and hsa-miR-196b-5p were enriched in mesenchymal stem cells and their derived tissues. In conclusion, our comparative miRNA profiling sheds light on differential expression patterns between SWR/J and both subgroups of TH. No differences were observed between TH and TH-ND, suggesting the genetic background of SWR/J may be responsible for the change of dysregulated miRNA.

Keywords: microRNA, type 2 diabetes, TallyHo, biomarker, next-generation sequencing, osteoporosis, circulating microRNA

Received: February 22, 2024. **Revised:** September 11, 2024. **Accepted:** September 16, 2024

Graphical Abstract

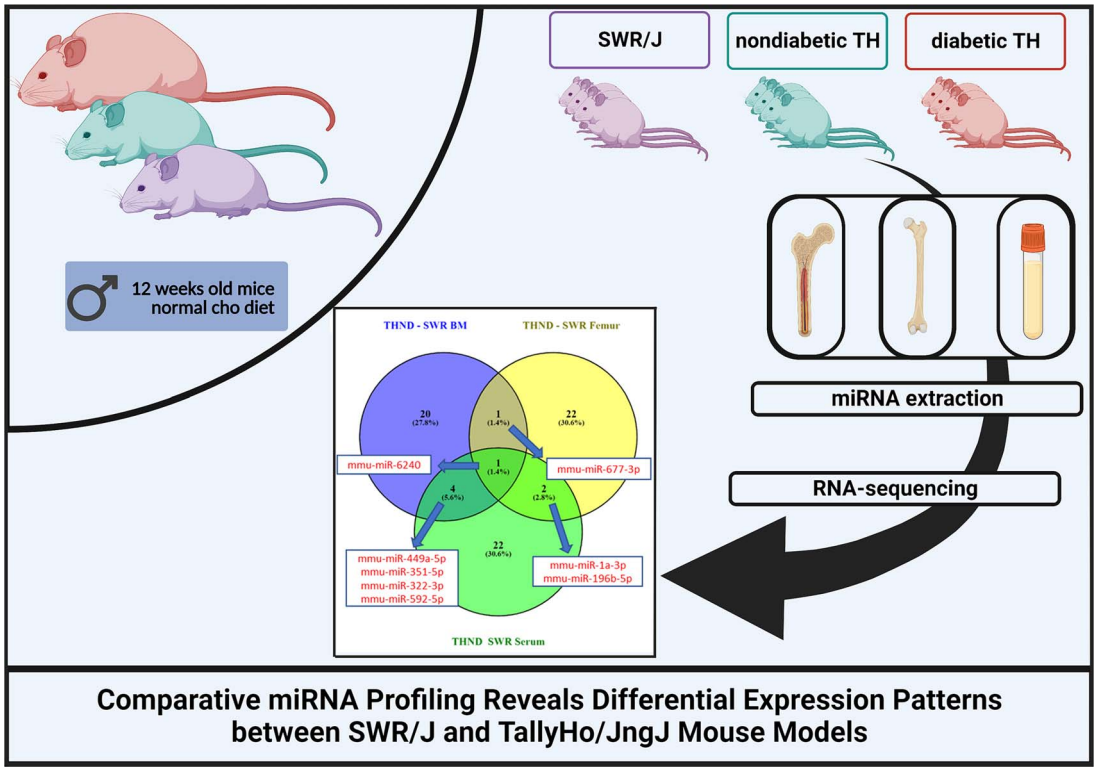

Introduction

Diabetes is well-defined by elevated blood glucose levels caused by a dysfunction in insulin metabolism. Type 1 diabetes mellitus (T1DM) is characterized by insufficient insulin production resulting from the autoimmune destruction of pancreatic islet beta cells.[1] In contrast, type 2 diabetes mellitus (T2DM) primarily arises from insulin resistance, often influenced by genetic predisposition, obesity, and an unhealthy lifestyle.[2] With the global prevalence of diabetes on the rise, an estimated 463 million people are affected, with T2DM accounting for ~90% of all cases.[3]

A range of late-stage complications accompany both forms of diabetes, including macro- and microvascular disease, retinopathy, and neuropathy.[4] Recently, studies have shown patients with T1DM and T2DM have an increased risk of fractures,[5] albeit through different mechanisms. While low BMD is the most common risk factor for patients with T1DM, patients with T2DM have normal or increased BMD.[6] This indicates that the diabetic bone quality is less resistant to fractures. This phenomenon is also known as the diabetic paradox of bone fragility, suggesting that other factors aside from BMD must contribute to the increased fracture risk in T2DM.

Substantial evidence has shown T2DM is linked to low bone turnover, leading to a failure to renew microdamage that naturally happens over time, resulting in the accumulation of bone that is structurally weak.[7] In addition, high levels of advanced glycation end-products (AGEs) may contribute to stiff collagen structures and altered bone cell functions in diabetic bone disease. Further, under diabetic conditions, bone formation is significantly impaired.[8] One contributing factor to decreased osteogenesis and increased adipogenesis in diabetic bone disease is the inhibition of Wnt signaling. Additionally, enhanced oxidative stress may hamper osteoblast function.[9–15]

More recently, microRNAs (miRNAs), short single-stranded non-coding RNAs that regulate gene expression at a transcriptional level,[16–19] have been shown to be dysregulated in diabetic bone disease in humans and in rodent models. We previously detected several dysregulated miRNAs in the serum and bone of ZDF rats, a monogenetic model of diabetic bone disease based on a mutation in the leptin receptor gene. Further, we found that these miRNAs are differently affected by bone-specific treatments such as anti-sclerostin antibodies (anti-scl) and parathyroid hormone (PTH), or insulin.[20]

A meta-analysis study reported 40 miRNAs to be significantly dysregulated in T2DM patients. This includes miR-375, miR-142-3p, and miR-144, along with 2 tissue miRNAs, miR-199a-3p and miR-233. Furthermore, another study investigated stress-related miRNA biomarkers in relation to T2DM and discovered that miR-148b, miR-223, miR-130a, miR-19a, and miR-26b are potential biomarkers for T2DM.[21,22]

To understand the role of miRNA in diabetic bone disease with a polygenetic perspective and assess if we would find similar miRNAs regulated as in monogenetic T2DM models, we aimed to analyze serum and bone tissue samples from TallyHo/JngJ mice. The TallyHo/JngJ strain is a polygenetic murine model that recapitulates T2DM with similar features as seen in humans. Previous studies have reported that they develop a bone phenotype characterized by reduced BMD, altered bone microarchitecture, and increased bone turnover when compared to SWR/J mice as their recommended control.[23–25]

Table 1. Summary of the animals used for the study.

Genotype	Serum	Bone (cortical)	Bone marrow	Total
TallyHo/JngJ	5	5	6	16
Strain-matched non-diabetic control	5	5	5	15
Swiss Webster Random/Jackson	5	4	5	14
Total	15	14	16	45

Serum, bone marrow, and cortical bones were collected from 11 male TallyHo/JngJ mice, 6 TH (diabetic) and 5 TH-ND (non-diabetic), and 5 male SWR/J mice at the age of 12-wk-old. Micro-CT, serum, and tissue analyses were performed as indicated in the paper submitted paper by Emini et al.[26]

In this study, we employed an untargeted profiling technique, next generation sequencing (NGS), to quantify miRNA levels in serum and ulna samples from TallyHo/JngJ. With the generated NGS, data we performed hierarchical clustering analysis, univariate and multivariate statistical analysis, as well as gene target network analysis and cell-type enrichment analysis to identify the most promising miRNA biomarker candidates for diabetic bone disease.

Materials and methods

Animals

Animal procedures were approved by the institutional Animal Care Committee of the Technische Universität Dresden and the Landesdirektion Sachsen (TVV 2017/20). Twelve-week-old male mice TALLHYHO/Jng and SWR/J were purchased from Jackson Laboratory and house under institutional guidelines. Animals were maintained in groups up to 5 animals in a light–dark cycle of 12/12 h at room temperature in filter-top cages and had ad libitum access to their respective drinking water and standard chow diet. Body weight measures, serum analysis, and assessment of bone mass and bone microarchitecture were performed at the TUD in all mice as described by Emini et al.[26]

To investigate changes in circulating and bone miRNA expression as a consequence of the TH-ND phenotype, serum, BM, and cortical bone samples were harvested at Week 12 at the Bone Lab located in the TUD (Technical University of Dresden, Germany) and used for RNA extraction. RNA extraction from cortical bone was performed at TUD, while RNA extraction from serum and BM and NGS were performed at TAmiRNA GmbH for a genome-wide screen of miRNA levels in a subset of 45 serum samples as shown in Table 1. BM and cortical bone tissue samples were collected from the same rats used for serum collection.

RNA extraction from serum and bone marrow

Total RNA was extracted from 100 μL serum and flushed bone marrow using the miRNeasy Mini Kit (Qiagen, Germany) as described by Kocijan et al.[27] 100 μL of each sample were mixed with 1000 μL of Qiazol and 1 μL of a mix of 3 synthetic spike-in controls (Exiqon, Demark). After a 10-min incubation at room temperature, 200 μL of chloroform were added to the lysates, followed by centrifugation at 12 000 $\times$ *g* for 15 min at 4 °C. 650 μL of the upper aqueous phase were transferred to a miR-Neasy mini column where RNA was precipitated with 750 μL ethanol, followed by automated washing with RPE and RWT buffer in a QiaCube liquid handling robot.

Finally, total RNA was eluted in 30 μL nuclease free water and stored at −80 °C. The RNA yield was analyzed for all samples. Due to low RNA concentrations in biofluids, which render most RNA quantifications inaccurate, serum RNA extraction efficiency was assessed through RT-qPCR analysis of spike-ins added prior to the RNA extraction step. Spike-in controls showed acceptable variation by RT-qPCR for all serum RNA samples, proving an acceptable quality for their use in further experiments. Microcapillary electrophoresis (Bioanalyzer, Agilent) was performed to determine the RNA concentration and the RNA integrity (RIN) in all tissue RNA samples. RNA quality was also high and remained stable among bone marrow RNA samples, as RIN values were in a range of 8.7-9.4 for all samples.

RNA extraction from cortical bone

Cortical bones were harvested from all mice, bone marrow was flushed, and the bone was homogenized with a mortar at the Bone Lab in the TUD (Dresden), and samples were immediately snap frozen in liquid nitrogen and stored at −80 °C. Total RNA from bone tissue was extracted using TRIzol reagent (Invitrogen, Darmstadt, Germany), respectively, following the manufacturer's protocol and quantified using a Nanodrop spectrophotometer (Peqlab, Erlangen, Germany). Similar to the bone marrow RNA samples, RNA concentration and RIN were determined for all cortical bone tissue RNA samples to confirm their quality. The quality of the cortical bone tissue RNA samples was lower than the one of bone marrow RNA samples, but similar to bone marrow samples, the RIN values remained stable among cortical bone RNA samples, as RIN values were in a range of 2.0-2.7 for all samples. All cortical bone tissue RNA samples were stored at −80 °C.

Library preparation for small RNA-Seq

Based on previous studies performed by Khamina et al.,[28] library preparation was performed using the RealSeq-Biofluids Plasma/Serum miRNA Library kit for Illumina sequencing (RealSeq Biosciences, 600-00048; protocol 20181220_RealSeq-BF_CL) according to the manufacturer's protocol. Briefly, 8.5 μL of extracted RNA were used as input, using the same RNA concentration (11.8 ng/μL) for all cortical bone tissue and bone marrow RNA samples. Adapter-ligated libraries were circularized, reverse transcribed and amplified.

Library PCR was performed with Illumina primers included in the kit and using 22 cycles for serum samples, 18 cycles for bone marrow samples, and 29 cycles for cortical bone tissue samples. In total, 15 miRNA libraries were prepared from serum samples, 14 miRNA libraries were prepared from cortical bone samples, and 16 from bone marrow samples.

All 45 libraries were analyzed for library fragment distribution using the Agilent DNA1000 kit (Agilent Technologies, 5067-1504) with Agilent DNA1000 reagents (Agilent Technologies, 5067-1505). The generated libraries were pooled in

an equimolar proportion, and the obtained pool was size-selected with the BluePippin system using a 3% agarose cassette with a target range of 100-250 kb (Sage Science, BDQ3010) to remove DNA fragments outside of the target range.

The pooled and purified libraries were analyzed for fragment distribution on an Agilent High Sensitivity DNA kit (Agilent Technologies, 5067-4626) with Agilent High Sensitivity DNA reagents (Agilent Technologies, 5067-4627). The library pool was then sequenced on an Illumina NextSeq550 (single-read, 75 bp) according to the manufacturer's protocol at the Vienna BioCenter Core Facilities (VBCF), Vienna, Austria.

RT quantitative polymerase chain reaction analysis

Starting from total bone marrow and serum RNA samples, cDNA was synthesized using the miRCURY LNA RT kit (Qiagen, Cat No. 339340). In total, 2 μL of total RNA were used for serum samples and 40 ng from bone marrow per 10 μL RT reaction. To monitor RT efficiency and presence of impurities with inhibitory activity, a synthetic RNA spike-in (cel-miR-39-3p) was added to the RT reaction.

PCR amplification was performed in a 96-well plate format using miRCURY SYBR Green qPCR (Qiagen, Cat No. 339347) and miRCURY LNA miRNA primers miR-592, miR-449a, miR-351-5p, and miR-322-3p (Qiagen Cat No. 339306). qPCR was performed in a Roche LC480 II instrument (Roche, Germany). All steps were performed according to the manufacturer's instructions.

To calculate the cycle of quantification values (Cq-values), the second derivative method was used. Spike-in control cel-miR-39-3p values were used for monitoring data quality and showed acceptable variation. Cq-values of endogenous serum miRNAs were normalized to the RNA spike-in controls by subtracting the individual miRNA Cq-value from the RNA spike-in Cq, thus obtaining delta-Cq (dCq) values that were used for the statistical analysis. Similarly, Cq-values of endogenous bone marrow miRNAs were normalized to the mean of 2 established reference RNAs—5S and SNORD65—by subtracting the individual miRNA Cq-value from the mean Cq of the references, thus obtaining delta-Cq (dCq) values that were also used for the statistical analysis.

Statistical analysis

Statistical differences in bone and metabolic phenotype between all groups of mice were conducted using GraphPad Prims v9.5.0. Statistical significance of group differences was assessed using 2-way-ANOVA in conjunction with Sidak tests for multiple comparisons.

Analysis of RNA-Seq data was performed with the software package MiND, a data analysis pipeline that generates overall QC data, unsupervised clustering analysis, normalized miRNA count matrices, and differential expression analysis based on raw NGS data.[29]

Overall quality of the next-generation sequencing data was evaluated automatically and manually with fastQC v0.11.9 and multiQC v1.10. Reads from all passing samples were adapter trimmed and quality filtered using cutadapt v3.3 and filtered for a minimum length of 17 nt. Mapping steps were performed with bowtie v1.3.0 and miRDeep2 v2.0.1.2, whereas reads were mapped first against the genomic reference GRCm38.p6 provided by Ensembl, allowing for 2 mismatches, and subsequently miRBase v22.1, filtered for miRNAs of mmu only, allowing for 1 mismatch. For a general RNA composition overview, non-miRNA mapped reads were mapped against RNA central and then assigned to various RNA species of interest.

Statistical analysis of preprocessed NGS data was done with R v4.0 and the packages espheatmap v1.0.12, pcaMethods v1.82, and genefilter v1.72. Differential expression analysis with edgeR v3.32 used the quasi-likelihood negative binomial generalized log-linear model functions provided by the package. The independent filtering method of DESeq2 was adapted for use with edgeR to remove low abundant miRNAs and thus optimize the false discovery rate (FDR) correction.

Regarding the RT-qPCR validation of NGS data, statistical differences in bone marrow and serum miRNA d-Cq values between TH-ND and SWR mice were also conducted using GraphPad Prims v9.5.0. The statistical significance of group differences was assessed using the Mann–Whitney test. Scatterplots present the distribution of values as well as mean $\pm$ SD.

Hierarchical clustering with the associated heatmap was performed with the ClustVis online tool using only miRNAs that show an RPM in at least $1/n$ (groups) percent of samples (eg, with 4 groups, the miRNA has to have an RPM value above 5 in at least 25% of the samples). This removes miRNAs that have a high CV but are only expressed in a too small amount of samples to bear any statistical significance or biological relevance.

RNA target network construction

The 7 miRNAs that were differentially dysregulated in both bone (either bone marrow or cortical bone tissue) and serum of TH-ND mice compared to SWR were used for constructing a target network using the online tool miRnet 2.0 (https://www.mirnet.ca/miRNet/upload/MirUploadView.xhtml). One miRNA (mmu-miR-6240) could not be identified by the miRNet 2.0 tool, but the remaining 6 miRNAs were mapped to their target mRNAs.

Genes listed in miRTarBase v8.0 and TarBase v8.0 repositories were selected for network construction. Of note, the miRTarBase v8.0 repository exclusively records experimentally verified miRNA–gene interactions. Therefore, the networks constructed by this tool are of relatively good robustness. After gene selection, the degree filter was set to 2; hence, only gene target nodes with at least 2 connections for the 6 miRNAs dysregulated in both bone and serum remained in the network.

The KEGG and Reactome databases were used for pathway enrichment, using all genes identified in the network and hypergeometrical testing. For each of the used databases, pathways of interest (with an FDR $< 20\%$) were selected based on their known role on bone biology or relation with bone quality and osteoporosis. For a simpler visualization of the network, all gene target nodes that were not present in the selected pathways of interest were hidden in the network.

Cell-type enrichment analysis

FANTOM (Functional Annotation of the Mouse/Mammalian Genome) is an integrated expression atlas of miRNAs. It uses sRNA sequencing data across a wide variety of humans and mice samples to create a miRNA expression

atlas for human and mouse, and annotates each miRNA based on its expression profile across cell types.[30] Using the FANTOM5 browser (https://fantom.gsc.riken.jp/5/suppl/De_Rie_et_al_2017/vis_viewer/#/about), we could find and visualize the expression profile of human mature miRNAs across tissues and cell types as measured in FANTOM5 and the cell ontology terms associated with each mature miRNA. For this, an average miRNA expression level was calculated for each cell type (regardless of the tissue of origin) that was available in the FANTOM5 database. Expression information from cells derived from male or female reproductive organs or cells obtained under a certain treatment were excluded from this analysis. We represented such an expression profile using hierarchical clustering with the associated heatmap, which was performed with the ClustVis online tool.

Results

Study design

TallyHo/JngJ mice ~25% spontaneously develop T2DM between the age of weeks 9 and 11 due to multiple susceptibility loci (quantitative trait loci) for diabetic complications,[31] whereas SWR/J mice and those TallyHo/JngJ that do not develop T2DM served as controls. Cryo-preserved serum, bone marrow, and bone tissue samples from 6 male TallyHo/JngJ mice with T2DM (TH), 5 nondiabetic TH mice also known as the strain-matched control (TH-ND), and 5 from the recommended control (SWR/J) mice were obtained. All animals that were used for this study had previously been investigated for their bone phenotype[26] (Table 1).

Animal phenotype analysis

The mouse phenotype has been re-analyzed from the data shown in the paper submitted by Emini et al.,[26] using the current no. of samples per group used for this study. Body weight (Figure 1A) did not significantly change in any group of TH mice compared to SWR/J control, but we observe a certain tendency to increase in both TH and TH-ND mice compared to SWR/J mice. Glucose (Figure 1B) was significantly increased in TH mice compared to SWR/J and TH-ND mice. Bone turnover was lower in both TallyHo/JngJ subgroups compared to SWR/J mice indicated by decreased levels of procollagen type I N-propeptide (P1NP) and tartrate-resistant acid phosphatase (TRAP) (Figure 1C and D). Analysis of femoral bones showed that cortical thickness and BMD were significantly increased in both TH and TH-ND mice compared to SWR/J mice (Figure 1E and F), while trabecular number and BMD were significantly decreased in both TallyHo/JngJ subgroups compared to SWR/J control mice (Figure 1G and H).

miRNA dysregulation in serum, bone marrow, and cortical bone tissue in the context of hyperglycemia in TallyHo/JngJ mice

NGS analysis was performed on all 16 bone marrow and 15 serum samples and 14 cortical bone samples obtained from TH, TH-ND, and SWR/J mice (Table 1). NGS data quality was checked based on total reads obtained per sample and relative reads mapping against miRNA reads (Figure S1A and B). After quality filtering and adapter trimming, the total read count ranged between 6 and 11 million reads for bone marrow samples, 4 and 13 million reads for serum samples, and 1.4 and 5 million reads for cortical bone samples. 40% of reads on average mapped against miRNAs in the bone marrow samples, while this percentage decreases to 7% in serum samples and to 3.5% in cortical bone samples.

Overall, more than 1500 distinct miRNAs (1604 miRNAs) were detected in bone marrow, serum, and cortical bone tissue, of which more than 750 miRNAs, 530 miRNAs, and 160 miRNAs were detected per bone marrow, serum, or cortical bone samples, respectively (Figure S1C, red bars). Of these more than 390 miRNAs, 230 miRNAs, and 100 miRNAs showed a read count of >10 reads per bone marrow, serum, and cortical bone sample, respectively (Figure S1C, green bars). First, we analyzed miRNA changes in bone marrow, serum, and cortical bone in 6 TH mice compared to 5 TH-ND mice using an adjusted p-value cut-off of .2 (FDR < 20%) to identify differentially expressed miRNAs. Out of the 1604 detected miRNAs, 386 bone marrow, 81 serum, and 122 cortical bone miRNAs were included in the analysis after filtering for low abundant miRNAs (Figure 2).

In the bone marrow of TH mice, we identified 5 significantly up- and 1 down-regulated miRNAs (Figure 2A) compared to TH-ND mice. In cortical bone, the same group comparison did not identify any significantly dysregulated miRNAs (Figure 2B). Last, in the serum of TH mice, we identified 3 significantly up- and 6 down-regulated miRNAs (Figure 2A) compared to TH-ND mice (Figure 2C). Among all miRNAs dysregulated in serum and in bone marrow of TH mice compared to TH-ND, only 2 miRNAs (mmu-miR-466i-5p and mmu-miR-1195) were found to be shared (up-regulated) in both compartments (Figure 2D). In serum, a $\log_2$ fold change ($\log_2$FC) of 3.7 (FDR = 0.15) and of 1.9 (FDR = 0.15) were observed for mmu-miR-466i-5p and mmu-miR-1195, respectively. In bone marrow, both miRNAs had a $\log_2$FC of 1.6 (FDR = 0.0023).

miRNA dysregulation in serum, bone marrow, and cortical bone tissue of non-diabetic TallyHo/JngJ mice compared to SWR/J control

To compare serum miRNA patterns in TH-ND vs SWR/J mice, unsupervised analysis of all serum samples was performed based on the expression values of the miRNAs among the 2 groups and for the 3 compartments (bone marrow, cortical bone, and serum) that show one read per million (RPM) in at least $1/n$ (groups) percent of samples (eg, with 4 groups, the miRNA has to have an RPM value above 5 in at least 25% of the samples). The heatmap and hierarchical clustering (Figure S2) showed a clear division and grouping of the samples based on their miRNA patterns between the analyzed compartments first and between genotypes within each compartment, indicating that miRNAs reflect each sample's genotype and compartment of origin.

Indeed, group-wise comparison showed that the different genetic background of TH-ND mice resulted in a significant (FDR < 0.2) regulation of 26 miRNAs (12 up, 14 down) in the bone marrow compared to SWR/J control mice (Figure 3A). Similar dysregulation is observed with significant changes (FDR < 0.2) of the levels of 26 miRNAs (10 up, 16 down) in the cortical bone of TH-ND mice compared to SWR/J mice

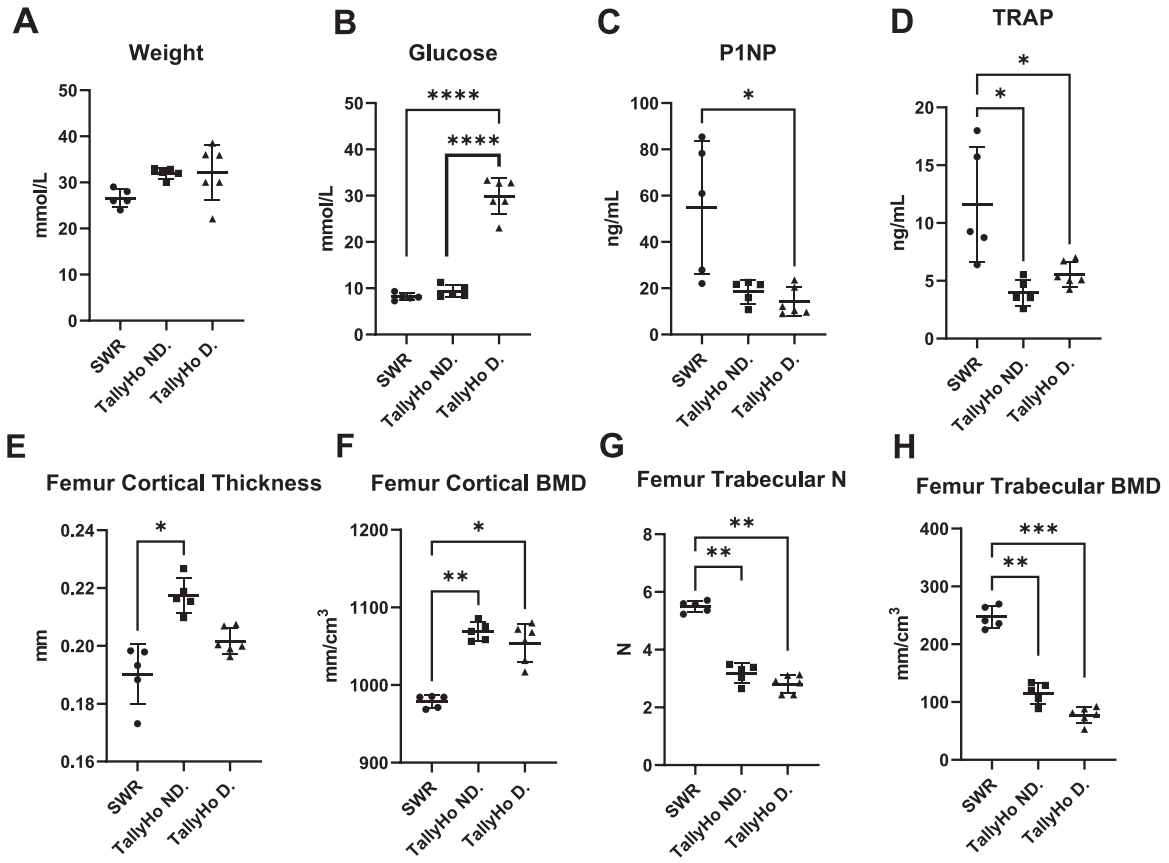

Figure 1. Re-analyzed characterization of animal phenotypes. Metabolic parameters (A-D), as well as femora bone parameters (E-H) were evaluated. *Ex vivo* micro-CT analysis were performed to determine BMD (TH $n = 6$; TH-ND $n = 5$; SWR $n = 5$). Scatter plots show mean ± SD. 2-way ANOVA analysis was performed. $p < .1$ shown in numeric values, $^{*}p < .05$, $^{**}p < .01$, $^{***}p < .001$, $^{****}p < .0001$.

(Figure 3B). The genetic background of TH-ND mice resulted in a further dysregulation of 29 miRNAs (14 up, 15 down) in serum compared to SWR/J mice (Figure 3C). When looking at the top 5 miRNAs with the highest dysregulations by $\log_2$FC (Table S1), we observed that the most dysregulated miRNAs are present in cortical bone, with mmu-miR-1895 and mmu-miR-677-3p showing a $\log_2$FC of -12 and -8, respectively. The top 5 miRNAs in serum show a $\log_2$FC between ±2 and ±3, while in bone marrow they show a $\log_2$FC between ±1 and ±2 except for mmu-miR-129-5p, with a $\log_2$FC of −4.2.

To identify which miRNA dysregulated in serum of TH-ND mice compared to SWR/J mice could potentially be used as a biomarker indicative of the lower bone quality of TH-ND mice, we overlapped those dysregulated circulating miRNAs in TH-ND mice with the miRNAs dysregulated in bone marrow and in cortical bone of TH-ND mice compared to SWR/J mice. By doing so, we identified 4 miRNAs (mmu-miR-449a-5p, mmu-miR-351-5p, mmu-miR-322-3p, and mmu-miR-592-5p) overlapping between the serum and the bone marrow compartments, meaning that they are dysregulated in both compartments in TH-ND mice, as shown on the left overlapping area of the VENN diagram (Figure 3D). Another 2 miRNAs (mmu-miR-1a-3p and mmu-miR-196b-5p) appear to be dysregulated in both cortical bone and serum of TH-ND mice, as shown in the right overlapping area of the VENN diagram (Figure 3D). On the upper area of the VENN diagram, one miRNA (mmu-miR-677-3p) was found to overlap between TH-ND vs SWR/J in the bone marrow and in the cortical bone tissue, suggesting a potential role in the whole bone of this miRNA (Figure 3D). Furthermore, only one miRNA (mmu-miR-6240) was found to be dysregulated in the 3 analyzed compartments, as seen in the central overlapping area of the VENN diagram.

Last, to check if some miRNAs dysregulated due to hyperglycemia in TH mice compared to TH-ND are among the miRNAs dysregulated in TH-ND compared to SWR/J, we overlapped those dysregulated circulating miRNAs in TH-ND vs SWR/J mice with the dysregulated circulating miRNAs in TH vs TH-ND mice (Figure S3). Three miRNAs that appeared to be upregulated by hyperglycemia in TH mice were also dysregulated in TH-ND mice compared to SWR/J but showing opposite trends since they were downregulated in TH-ND mice. In bone marrow, no overlap was found, indicating that the 6 miRNAs dysregulated by hyperglycemia in TH mice compared to TH-ND are not among the 26 dysregulated miRNAs in TH-ND compared to SWR/J.

Last, for reproducibility purposes, we performed RT-qPCR on the 4 miRNAs (mmu-miR-449a-5p, mmu-miR-351-5p, mmu-miR-322-3p, and mmu-miR-592-5p) dysregulated in both the serum and the bone marrow compartments of TH-ND mice compared to SWR control mice. Briefly, NGS results for bone marrow could be replicated (Figure S4A-D), while for serum, the 2 circulating miRNAs with FDR < 0.05 in the NGS data (miR-592-5p and miR-449a-5p) were also

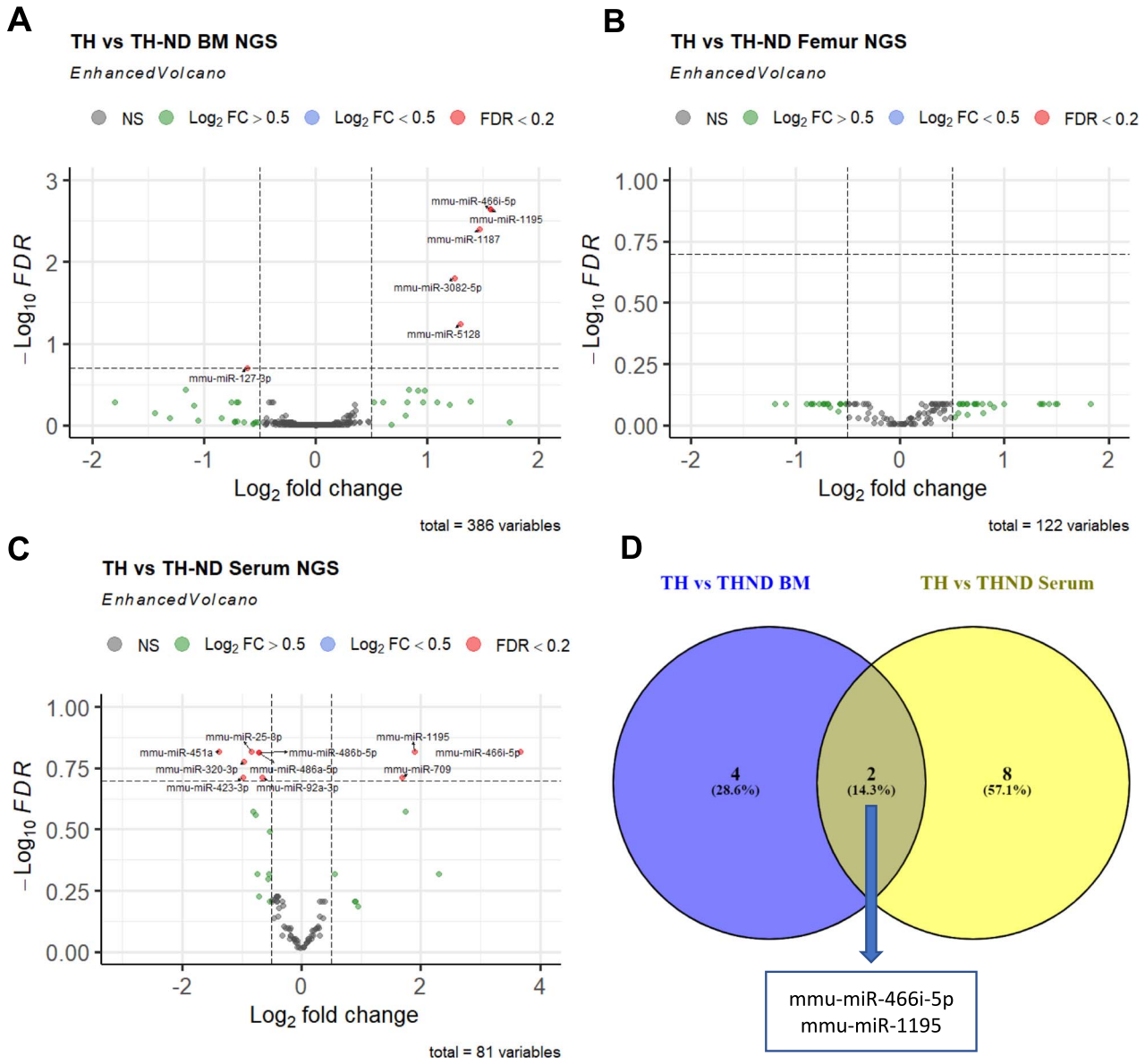

Figure 2. NGS-based discovery of miRNA changes in serum and bone marrow of TH mice compared to TH-ND mice. (A-C) Volcano plots depict the log_2 transformed fold change and log10 transformed adjusted *p*-values for the contrast (TH $n = 6$; TH-ND $n = 5$) in bone marrow, cortical bone tissue and serum compartments. miRNA effects with Benjamini-Hochberg adjusted *p*-values <0.2 (FDR < 20%) are highlighted as a separate group with their annotated names. (D) Comparison of miRNAs dysregulated in serum and in bone marrow (FDR threshold of 0.2). VENN diagram with the overlapping miRNAs between the two compared lists corresponding to the miRNAs dysregulated in the TH model in bone marrow (left circle) and serum (right circle). mmu-miR-466i-5p and mmu-miR-1195 that are dysregulated in the TH model in both compartments are in the overlapping area of the circles.

confirmed (Figure S5A and B). The other 2 circulating miRNAs (miR-351-5p and miR-322-3p) were not significantly dysregulated in TH-ND mice compared to SWR mice (Figure S5C and D).

miRNAs generally show same tendencies of dysregulation when dysregulated in 2 or 3 of the analyzed compartments

Out of the 5 dysregulated miRNAs in both bone marrow and serum of TH-ND mice compared to SWR/J mice, 1 (mmu-miR-592-5p) showed opposite tendencies of dysregulation (upregulated in bone marrow and downregulated in serum of TH-ND mice), while 4 (mmu-miR-449a-5p, mmu-miR-351-5p, mmu-miR-322-3p, and mmu-miR-6240) showed the same tendencies of dysregulation in both compartments, with 2 upregulated and 2 downregulated in both bone marrow and serum of TH-ND mice when compared to SWR/J control (Figure 4A-E and Table 2).

Out of the 3 dysregulated miRNAs in both cortical bone tissue and serum of TH-ND mice compared to SWR/J mice, 1 (mmu-miR-196b-5p) showed opposite tendencies of dysregulation (downregulated in cortical bone and upregulated in serum of TH-ND mice), while 2 showed the same tendencies of dysregulation in both compartments, with 1 downregulated (mmu-miR-6240) and 1 upregulated (mmu-miR-1a-3p) in both cortical bone tissue and serum of TH-ND mice when compared to SWR/J control (Figure 4E-G and Table 2). Of

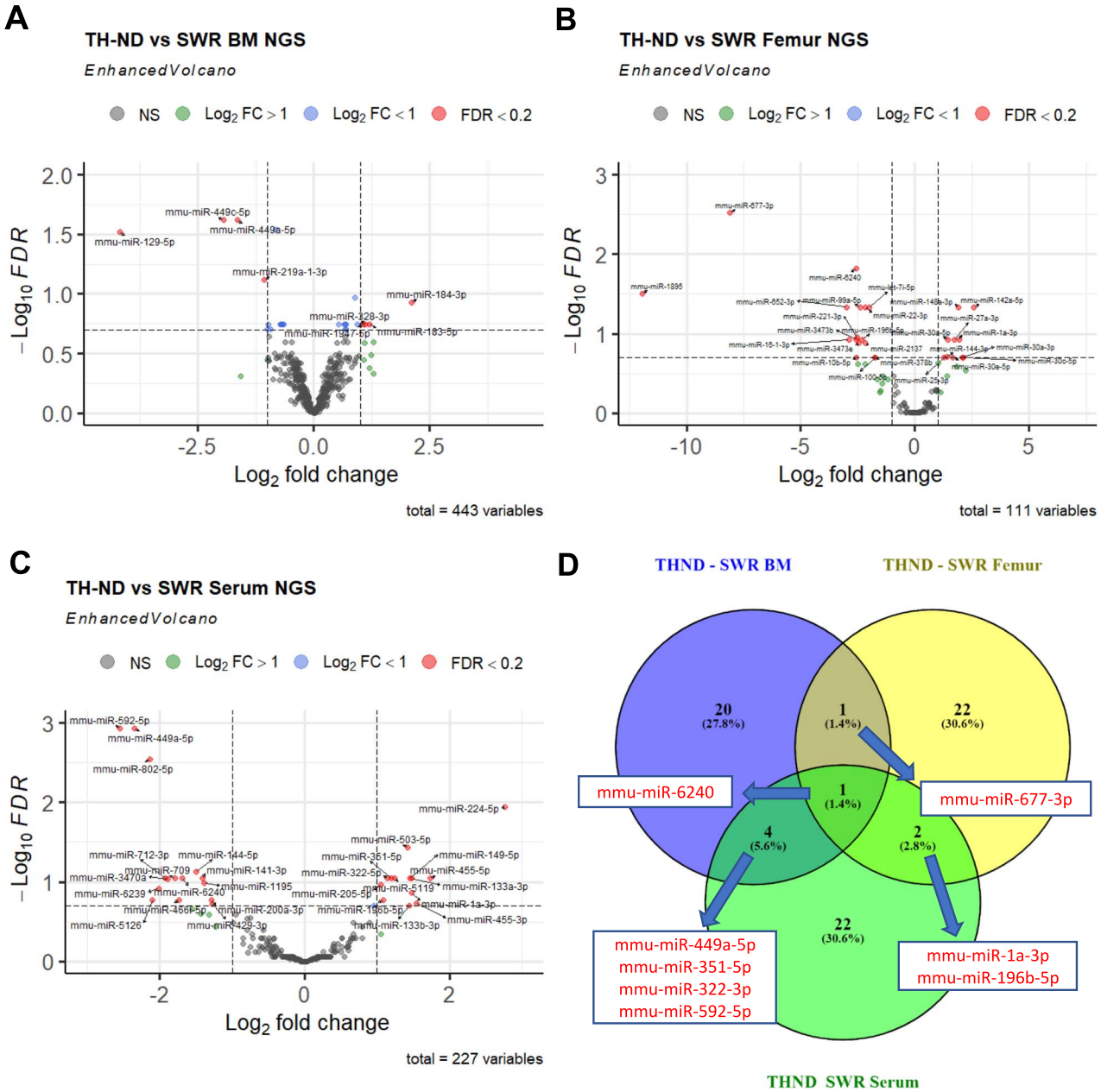

Figure 3. NGS-based discovery of miRNA changes in bone marrow, cortical bone tissue and serum of TH-ND mice compared to SWR mice. (A-C) Volcano plots depict the $\log_2$ transformed fold change and log10 transformed adjusted *p*-values for the contrast (TH-ND mice $n = 5$ vs SWR mice $n = 5$) in bone marrow, cortical bone tissue and serum. miRNAs with Benjamini–Hochberg adjusted *p*-values < .2 (FDR < 20%) are highlighted as a separate group with their annotated names. (D) VENN comparison of miRNAs dysregulated in bone marrow (left circle), cortical bone tissue (right circle) and serum (bottom circle) of TH-ND vs SWR (FDR < 20%). miRNAs that are dysregulated in 2 or more compartments are highlighted with their annotated names.

note, mmu-miR-6240 was the only miRNA dysregulated in the 3 analyzed compartments and showing the same tendencies in all of them, being downregulated in bone marrow, cortical bone, and serum of TH-ND mice compared to SWR/J mice (Figure 4E and Table 2).

Finally, mmu-miR-677-3p was the only miRNA to be dysregulated in just both bone marrow and cortical bone of TH-ND mice compared to SWR/J mice, showing the same tendencies since it is downregulated in both compartments (Figure 4H and Table 2).

In order to investigate the cellular origin and putative biological function of miRNAs found to be dysregulated in serum as well as in bone tissue, we analyzed miRNA tissue enrichments and constructed mRNA target interaction networks.

Gene target and network analysis comprises pathways involved in bone biology potentially targeted by the dysregulated miRNAs in both bone and serum of TH-ND mice

In order to obtain a miRNA-targeted gene network, we used the 7 miRNAs that were differentially dysregulated in both bone (either bone marrow or cortical bone tissue) and

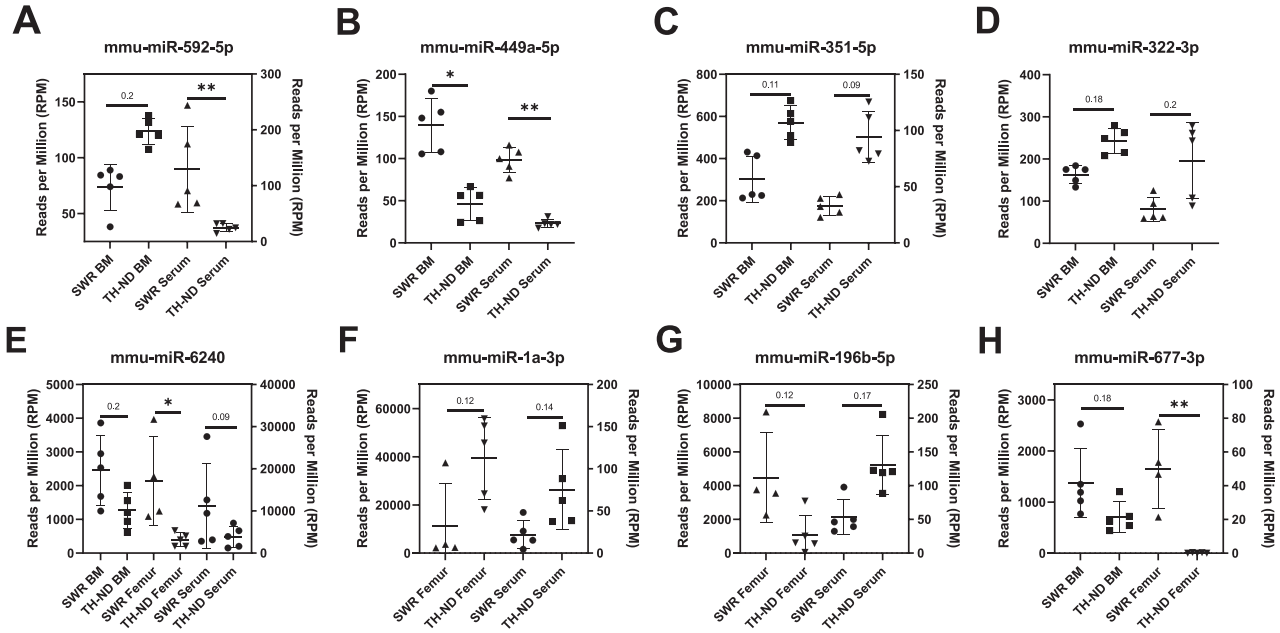

Figure 4. MicroRNA scatter plot representations of miRNAs shown by NGS to be dysregulated in 2 or 3 compartments. Scatter plots of the NGS data showing the differential expression of miRNAs dysregulated in both bone marrow and serum (A-E), cortical bone tissue and serum (E-G) and bone marrow and cortical bone (H) of TH-ND mice compared to SWR/J control mice. SWR/J bone marrow, $n = 5$; TH-ND bone marrow, $n = 5$, SWR/J serum, $n = 5$; TH-ND serum, $n = 5$; SWR/J cortical bone, $n = 4$; TH-ND cortical bone, $n = 5$. Scatterplots show mean ± SD. Right *y*-axis indicated the RPM measures for serum and cortical bone compartments, while left *y*-axis indicates RPM measures for bone marrow. Testing was performed using edgeR as described in the method section. FDR < 0.1 shown in numeric values, * FDR < 0.05, ** FDR < 0.01.

Table 2. Cross-sectional regulation among compartments of the miRNAs dysregulated in 2 or 3 compartments.

	TallyHo ND vs SWR Bone marrow		TallyHo ND vs SWR Cortical bone		TallyHo ND vs SWR Serum	
miRNA	**Log_2FC**	**FDR**	**Log_2FC**	**FDR**	**Log_2FC**	**FDR**
mmu-miR-592-5p	0.6947	0.2	**Not detected**		−2.55	0.0012
mmu-miR-449a-5p	**−1.655**	**0.024**	**Not detected**		**−2.353**	**0.0012**
mmu-miR-351-5p	**0.8832**	**0.11**	**Not detected**		**1.198**	**0.09**
mmu-miR-322-3p	**0.5339**	**0.18**	**Not detected**		**0.9582**	**0.2**
mmu-miR-6240	**−0.9982**	**0.2**	**−2.572**	**0.015**	**−1.695**	**0.09**
mmu-miR-1a-3p	0.114	0.96	**1.92**	**0.12**	**1.481**	**0.14**
mmu-miR-196b-5p	0.3494	0.36	**−2.318**	**0.12**	1.086	0.17
mmu-miR-677-3p	−0.9816	0.18	**−8.09**	**0.003**	Not detected	

Differential expression of miRNAs dysregulated in both bone marrow and serum, cortical bone and serum, and bone marrow and cortical bone of TH-ND mice compared to SWR/J control mice (TH-ND mice, $n = 5$; SWR/J mice, $n = 5$). MiRNAs showing the same dysregulation tendencies in serum and in bone marrow or cortical bone tissue are highlighted in bold. Abbreviations: Log_2FC, log_2 fold change; FDR, false discovery rate.

serum of TH-ND mice compared to SWR/J (Figure 3D) to their experimentally confirmed target mRNAs using miRNet 2.0. One miRNA (mmu-miR-6240) was excluded due to a lack of experimentally confirmed targets. The resulting list of gene-miRNA interactions was filtered for genes with at least 2 gene-miRNA interactions, narrowing down this list to 41 targeted genes. Next, pathway enrichment analysis was performed on this list of genes based on the KEGG, Reactome and DisGeNET classifications to explore known biological pathways and diseases in which the targeted genes are involved. From the list of enriched (FDR < 0.2) pathways, we selected those relevant to bone biology and bone disease ("pathways of interest") and identified 13 target genes in the pathways of interest (Figure 5, Table 3).

MiR-592-5p did not show any interaction with any mRNA target present in the pathways of interest (Figure 5). Prominent genes were detected based on the KEGG classification, such as Myc, Ccnd1, Ccnd2, and Bcl2, which play important roles in Wnt, Hippo, and Jak–STAT signaling. When using the Reactome classification in the pathway enrichment analysis, we detected target genes like Itpr1 and Gab1, which are involved in insulin secretion, the Ca2+ pathway, and signaling by Wnt (Table 3).

Cell-type enrichment analysis reveals distinct putative donor cell types of the dysregulated and rescued miRNAs in ZDF rats

In order to explore the potential cellular origin of the circulating (serum) miRNAs dysregulated in TH-ND mice compared to SWR mice, we obtained miRNA expression profiles across a large variety of cell types in humans using the FANTOM5

Table 3. Pathway enrichment using the KEGG, Reactome, and DisGeNET databases.

Database	Pathway	Hits	*p*-value	FDR
KEGG	Focal adhesion	Bcl2, Ccnd1, Ccnd2, Met, Flt1	.00019	0.0031
	PI3K-Akt signaling pathway	Bcl2, Ccnd1, Myc, Ccnd2, Met, Flt1	.00025	0.0035
	Jak–STAT signaling pathway	Bcl2, Ccnd1, Myc, Ccnd2	.0008	0.0066
	Thyroid hormone signaling pathway	Ccnd1, Myc, Atp1b1	.0036	0.019
	Wnt signaling pathway	Ccnd1, Myc, Ccnd2	.0065	0.031
	Hippo signaling pathway	Ccnd1, Myc, Ccnd2	.0078	0.035
	Prolactin signaling pathway	Ccnd1, Ccnd2	.017	0.049
	ErbB signaling pathway	Myc, Gab1	.023	0.061
	HIF-1 signaling pathway	Bcl2, Flt1	.034	0.082
	AMPK signaling pathway	Ccnd1, Eef2	.047	0.099
	FoxO signaling pathway	Ccnd1, Ccnd2	.05	0.1
	Rap1 signaling pathway	Met, Flt1	.11	0.19
	Mineral absorption	Atp1b1	.12	0.19
Reactome	Semaphorin interactions	Met, Myh9	.016	0.13
	Elevation of cytosolic Ca2+ levels	Itpr1	.027	0.13
	Signaling by VEGF	Flt1, Itpr1	.038	0.13
	GLP1 regulates insulin secretion	Itpr1	.04	0.13
	DAP12 signaling	Itpr1, Gab1	.076	0.13
	Signaling by EGFR	Itpr1, Gab1	.086	0.14
	DAG and IP3 signaling	Itpr1	.095	0.14
	Ca2+ pathway	Itpr1	.095	0.14
	Iron uptake and transport	Slc22a17	.13	0.15
	Signaling by Wnt	Itpr1, Sox4	.17	0.17

Several pathways significantly enriched with an adjusted p value < .2 (FDR < 20%) were identified for 6 of the 7 dysregulated miRNAs in both bone (either bone marrow or cortical bone tissue) and in serum. Abbreviation: FDR, false discovery rate.

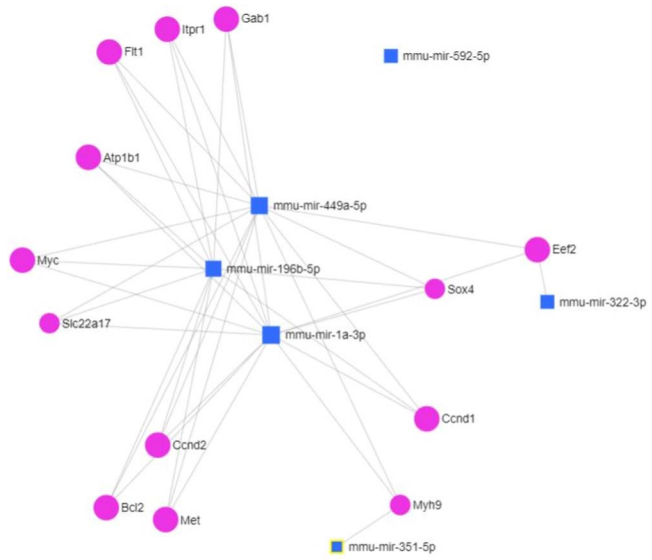

Figure 5. Target analysis of miRNAs dysregulated in bone and in serum (Table 2) using miRnet. Six out of seven miRNAs identified as significantly dysregulated in both bone (either bone marrow or cortical bone tissue) and serum of TH-ND mice compared to SWR/J mice could be used for constructing a target network using the online tool miRnet with a degree filter set to 2.

public data resource and visualized the data in the form of a heatmap (Figure 6). miR-6240 and miR-351-5p were excluded from the analysis because no data were available, as these 2 miRNAs are not annotated or conserved in humans. For each of the dysregulated miRNAs, all cell types with their respective miRNA average expression value (CPM, count per million) were selected.

We observe that the dysregulated miRNAs in TH-ND mice tended to group according to the cell lineage (Figure 6). Regarding the miRNAs dysregulated in both bone (either bone marrow or cortical bone tissue) and serum, they do not cluster together in the heatmap. From the miRNAs dysregulated in bone marrow and serum of TH-ND mice, hsa-miR-449a (homolog to mmu-miR-449a-5p) is mainly enriched in dendritic cells and T-lymphocytes, hsa-miR-592 is enriched in hepatocytes and in endothelial cells, and hsa-miR-424-3p (homolog to mmu-322-3p) is highly expressed in cells like hepatic stellate cells and the pituitary gland, but also in skeletal muscle cells and, to certain extent, mesenchymal stem cells (Figure 6). From the miRNAs dysregulated in both cortical bone and serum, hsa-miR-1-3p (homolog to mmu-miR1a-3p) is highly expressed in both skeletal muscle cells and myoblasts, while hsa-miR-196b-5p is enriched in renal mesangial cells, but also highly expressed in skeletal muscle cells and osteoblasts (Figure 6).

Discussion

We hypothesized that dysregulation of miRNA expression in bone tissue and bone marrow, as well as systemic dysregulation in serum, could be relevant to the phenotype observed in the polygenetic TallyHo/JngJ murine model of T2DM. Therefore, we used small RNA-sequencing analysis for untargeted characterization of miRNA levels in serum, cortical bone tissue, and bone marrow samples from TallyHo/JngJ with and without diabetes and also from its recommended control, the SWR/J.

miRNA dysregulation in all 3 compartments in the context of hyperglycemia in TallyHo/JngJ mice

Since for the 3 murine groups we wanted to demonstrate the miRNA profiles in circulation as well as in bone marrow and cortical bone tissue, we separated both tissues by flushing the bone marrow from the bones, leaving the cortical bone tissue

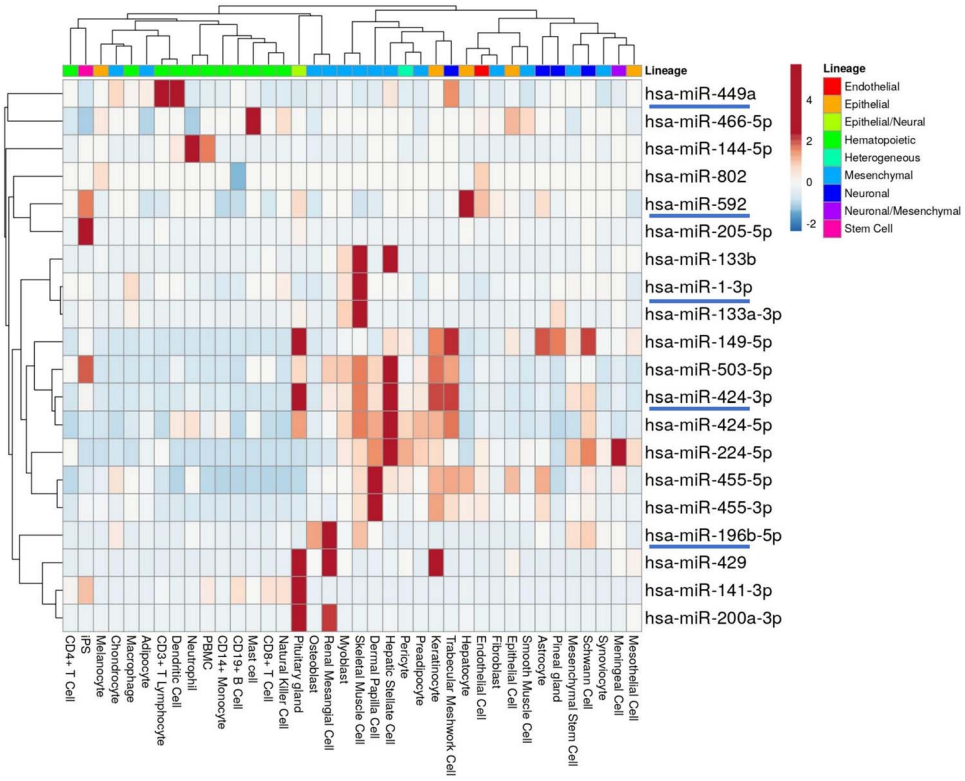

Figure 6. Heatmap illustrating the cellular expression profiles of circulating miRNA significantly dysregulated in TH-DN compared to SWR mice. The average miRNA expression levels of each cell type that appears in the FANTOM5 database were obtained and used to draw this heatmap. MicroRNAs that are dysregulated in both bone (either bone marrow or cortical bone tissue) and serum are highlighted in the figure. No data were available for miR-6240 and miR-351-5p in FANTOM5.

totally clean and ready for RNA extraction as described in the methods section.

A total of 1604 distinct miRNAs were detected in the serum, bone marrow, and bone tissue in the TH. However, among all the dysregulated miRNAs in the serum and in the bone marrow of TH, only 2 miRNAs (mm-miR-466i-5p and mm-miR-1195) were found to be shared (upregulated) in both compartments. Further, the cortical bone tissue revealed no difference in terms of dysregulated miRNA between the TallyHo/JngJ groups.

Previously, miR-466 expression was reported to be significantly upregulated in endothelial cells isolated from diabetic subjects compared to healthy subjects. In addition, *in vitro* studies have shown that the exposure of endothelial cells from healthy subjects to elevated glucose levels resulted in increased expression of miR-466.[32] Bioinformatic analysis and luciferase assays showed that miR-466 targets the 3′-untranslated region of the insulin receptor substrate 1 (IRS1) gene, thus regulating IRS1 mRNA and protein expression levels.[33] IRS1 is a critical element of the insulin-signaling pathway and may influence susceptibility to T2DM-related traits.[34] The specific role of miR-466 in diabetic bone disease is not fully understood and is still being explored. One study examined its role in wound healing. Bone marrow-derived progenitor cells (BMPCs) were isolated from adult subjects with and without T2DM. The study found that the transducer inositol-requiring enzyme 1α (IRE1α), which is a key protein involved in the cellular stress response, was significantly reduced in the diabetic condition. This reduction in IRE1α levels led to an overexpression of miR-466. The elevated levels of miR-466 subsequently inhibited the production of angiopoietin 1 (ANGPT1), a protein essential for the formation and stabilization of new blood vessels (angiogenesis). This impairment of angiogenesis negatively affects wound healing.[35]

In addition to miR-466 playing a vital role in angiogenesis, one study did show miR-1195 plays an important role in regulating adipogenesis and supports the balance between adipocyte and osteoblast differentiation; however, future studies are needed to understand its role in diabetic bone disease.[36] The RNA-sequencing analysis suggests miR-466i-5p and mi-miR-1195 are involved in the regulation of hyperglycemia and diabetes, though their role in bone is not fully understood, which is also very fitting with the lack of the different bone phenotypes we observed between these 2 models.

miRNA dysregulation in serum, bone marrow and cortical bone tissue of non-diabetic TallyHo/JngJ mice compared to SWR/J control

In our comparison between diabetic TH and TH-ND, only 2 miRNAs overlapped in both serum and bone marrow. None were found to overlap in all 3 compartments. However, comparison between TH-ND and SWR/J showed dysregulated miRNA in serum, bone marrow, and bone tissue. We identified 4 main miRNAs (mmu-miR-449a-5p, mmu-miR-351-5p, mmu-miR-322-3p, and mmu-miR-592-5p) that both were dysregulated in serum and bone marrow.

To evaluate the reproducibility of our NGS data, we replicated the analysis of these miRNAs by RT-qPCR in bone marrow and serum RNA samples. Indeed, RT-qPCR analysis

reproduced the results for bone marrow (Figure S4A-D) as well as for circulating miR-592-5p and miR-449a-5p, which showed FDR < 0.05 in the NGS data (Figure S5A and B). The other 2 circulating miRNAs (miR-351-5p and miR-322-3p) were not significantly dysregulated in TH-ND mice compared to SWR (Figure S5C and D). However, this is in line with the serum NGS data, where we did not observe FDR < 0.05 for these 2 circulating miRNAs. Overall, these new data are supportive of the robustness of the NGS data.

Unlike in bone marrow, we were not able to identify a dysregulation of mmu-miR-351-5p in cortical bone tissue, since this miRNA was not detected by NGS in half of the cortical bone samples. However, overexpression of mmu-miR-351 has been reported to be an inhibitor of alkaline phosphatase (ALP), collagen type II, osteopontin (OPN), and runt-related transcription factor 2 (RUNX2), genes that are specific for osteoblastogenesis.[37] The role of mmu-miR-592-5p has been linked to obesity. It was found to be significantly downregulated in the hepatic tissue of obese mice, correlating with hyperglycemia and insulin resistance, indicating compromised ability to regulate glucose homeostasis. Their functional assays demonstrated that overexpression of mmu-miR-592-5p ameliorated metabolic dysfunctions, leading to improvements in both insulin sensitivity and hyperglycemia. These findings indicate that miR-592 plays a protective role in maintaining metabolic homeostasis, and its deficiency contributes to the pathogenesis of diabetes by disrupting glucose and lipid metabolism.[38]

High reactive oxygen species (ROS) production and changes in cellular homeostasis link T2DM to oxidative stress.[39] Mitochondria, the primary source of ROS, increases ROS production when glucose levels are elevated, leading to oxidative stress and tissue damage.

mmu-miR-449a-5p was not found to be dysregulated in bone in our results; however, 1 study showed that mmu-miR-499a-5p plays a crucial role in regulating the expression of LIG3 and POLG1, both of which are essential for maintaining mitochondrial DNA integrity and function.[39] While no studies have specifically linked mmu-miR-449-5p to diabetic bone disease, existing research has demonstrated that mitochondrial dysfunction in bone cells plays a significant role in the pathogenesis of osteoporosis, leading to bone loss. Consequently, it is plausible that the regulation of LIG3 and POLG1 by mmu-miR-499a-5p could be disrupted due to the mitochondrial dysfunction associated with diabetes. This disruption may contribute to the observed bone loss in diabetic patients. Additionally, the role of mmu-miR-499a-5p has been associated with changes in the hypoxic environment, which could further influence its regulatory functions. Therefore, further studies are needed to investigate this potential.[40]

Both (mmu-miR-1a-3p and mmu-miR-196b-5p) were found to be dysregulated in bone tissue and serum. The physiological relevance of both miRNAs in diabetic bone disease has not yet been fully elucidated. However, mmu-miR-196b-5p plays an important role in insulin metabolism.

A study provides valuable insights into the regulation of insulin metabolism. Mmu-miR-196b-5p targets the 5′UTR of the insulin2 gene in mice and regulates insulin translation in an Argonaute 2 (Ago2)-dependent manner. This regulation occurs as part of the miRNA-induced silencing complex, which silences inhibitory proteins to facilitate insulin translation.[41] Targeting miR-196b or its associated pathways could potentially enhance insulin production in diabetic patients, thereby improving glucose homeostasis. This approach holds promise not only for managing diabetes but also as a future treatment for diabetic bone disease. Improving insulin regulation may help mitigate the adverse effects of diabetes on bone health, though extensive research is needed to fully understand the role miRNA plays in diabetic bone disease.

Mmu-miR-677-3p was discovered to be the only miRNA showing significant downregulation in bone marrow and bone tissue when comparing TH-ND to SWR/J.

Recent work suggests that mmu-miR-677-3p abundance increases in exosomes of mineralized osteoblasts and is considered as a potential miRNA biomarker in osteoporosis. Our results may indicate that mmu-miR-677-3p could also qualify as a biomarker of diabetic bone disease.[42,43]

The comparison between TH and TH-ND revealed no dysregulated miRNAs in cortical bone tissue. However, when comparing TH-ND to SWR/J, a single miRNA, mmu-miR-6240, was found to be dysregulated across serum, cortical bone, and bone marrow. Of note, this was the only miRNA that was downregulated in both cortical bone and bone marrow. The observed discordance in miRNA regulation across the investigated sample types indicates the distinct miRNA profiles and control mechanisms of miRNA transcription in bone marrow and in cortical tissue. This could be due to the different cellular composition, one being the bone niche while the other being mainly composed by osteocytes and bone matrix. This is further supported by the fact that within a given group, bone marrow and cortical bone tissue did not show an overlap in terms of miRNA profile, as expected due to the different cell type content of these 2 distinct, even if biologically interconnected, tissues. This lack of miRNA profile overlap can be seen in Figure S2, where the heatmap shows a clear separation between tissues and genotypes across all samples based on their whole miRNA profiles.

Interestingly, no studies have reported the role of mmu-miR-6240 in the context of bone fragility and T2DM, raising potential questions about its function. Overall, we suggest that the genetic background of TH-ND may be responsible for the significant change of dysregulated miRNA we observed compared to SWR/J. This was further supported by the lack of dysregulated miRNA in the bone tissue between TH and TH-ND, explained by sharing the same genetic background.

Finally, with relation to hyperglycemia, the 6 identified miRNAs in TH vs TH-ND in bone marrow were not among the 26 dysregulated miRNAs in TH-ND vs SWR/J, suggesting that none of the dysregulated miRNAs are responsible for the low bone quality we observed in diabetic TH, further supporting the lack of understanding of the role of hyperglycemia in this context.

Our study also revealed the 3 miRNAs that were up-regulated by hyperglycemia in TH mice, whereas they were among the 29 miRNAs that were down-regulated in TH-ND mice compared to SWR/J, indicating that the effect of hyperglycemia in TH may not be involved in the reduced bone quality of TH and TH-ND compared to SWR/J mice.

Epigenetics could play a role inducing the worse bone quality found in diabetic TH compared to SWR/J mice, regardless of the diabetic status. Another interesting finding we

discovered was that among the 29 circulating miRs that were dysregulated in TH-ND, we can potentially have a paracrine effect on the bone tissue of TH-ND and its reduced bone quality compared to SWR/J. For instance, circulating miR-802-5p was upregulated in ZDF rats while it is downregulated in TH-ND mice, being among the top 5 dysregulated miRNAs in serum of TH-ND compared to SWR/J (Table S1). Interestingly, circulating miR-320-3p was also dysregulated in ZDF rats (upregulated vs downregulated in TH mice vs TH-ND), and it was likely released from bone tissue.[20] This further raises the questions regarding miRNA being used as biomarkers for the indication of low bone quality.

miRNAs generally show same tendencies of dysregulation when dysregulated in 2 or 3 of the analyzed compartments

Our hypothesis of an epigenetic driven decrease in the bone quality of TallyHo/JngJ mice (regardless of diabetes) compared to SWR/J by miRNA is supported by the high miRNA dysregulation in bone and bone marrow of TH-ND mice compared to SWR/J control. The dysregulation of 4 out of 5 miRNA in the bone marrow of TH mice compared to SWR/J is reflected as well in the circulation, where they show the same tendencies (except miR-592-5p), making these miRNA interesting potential candidates as circulating biomarkers for low bone quality in TH mice. Further, of the 3 miRNAs that were dysregulated in both bone tissue and serum, 2 show the same tendencies in both compartments. miR-6240 is the only 1 dysregulated in the 3 compartments, showing the same tendency in all.

Gene target network analysis comprises pathways involved in bone biology potentially targeted by the dysregulated miRNAs in both bone and serum of TH-ND mice

By mapping 7 miRNAs that were dysregulated in both bone tissue (either bone marrow or bone tissue) and serum of TH-ND mice compared to SWR/J, we were able to create a miRNA-targeted gene network.

Myc, Ccnd1, Ccnd2, and Bcl1 were identified as target genes of 6 miRNAs. These genes usually play a significant role in the hippo pathway, Jak–STAT pathway, and the Wnt signaling pathway, with all of them being relevant to bone biology and bone diseases. Therefore, we believe these 6 miRNAs may have a potential role in decreasing the bone quality in diabetic TH mice, though future studies are needed to confirm if the actual cause of low bone quality is entirely contributed by the miRNA.

Cell-type enrichment analysis reveals distinct putative donor cell types of the dysregulated and rescued miRNAs in TH-ND mice

Circulating miRNAs can, in principle, originate from any cell type. However, ∼5%-10% of all miRNAs are transcribed at higher levels in only a few cell types, resulting in cell-type-specific miRNAs ("cell-type enrichment"). In order to determine a putative cellular origin of miRNAs dysregulated in serum, we retrieved the cell expression profiles as well as the associated cell ontology terms for all significantly dysregulated circulating miRNAs identified in this study from the FANTOM5 human database (Figure 6). According to miRNA expression, we observe as expected the clustering of the samples (cell types) toward their cell lineage, since gene expression generally is tissue-type specific.

The bone marrow is highly vascularized. Its vessels act as gates for hematopoietic niches and the blood to exchange information, cell nutrients, and waste products. Fitting with the dysregulation in serum but also in the bone marrow of TH-ND mice, hsa-miR-449a, a homolog to mmu-miR-449a-5p, is mainly enriched in cells, such as dendritic cells and T-lymphocytes. The hsa-miR-592 is mainly enriched in endothelial cells, and the hsa-miR-424-3p homolog to mmu-322-3p is highly expressed in skeletal muscle cells and, to some extent, in mesenchymal stem cells, also known to be present in the bone marrow as part of the bone niche (Figure 6).

The miRNAs dysregulated in both cortical bone tissue and serum, hsa-miR-1-3p homolog to mmu-miR1a-3p and hsa-miR-196b-5p, appear to be highly expressed in bone and its connected tissue, such as skeletal muscle. hsa-miR-1-3p is highly expressed in skeletal muscle cells, while hsa-miR-196b-5p is highly expressed in skeletal muscle cells and osteoblasts (Figure 6).

Contribution to the field and limitations of this study

To our knowledge, this is the first report on the role of miRNA in diabetic bone disease with a polygenic perspective. In this study, we described the involvement of specific miRNA in T2DM-induced bone disease. We further show a potential link between miRNA dysregulation in the circulation and in the bone tissue, with a potential prospect of using these miRNAs as a biomarker for diabetic bone disease.

The TallyHo/JngJ mice are a polygenic mouse model that naturally develops obesity and T2DM. These polygenic models of obesity may provide a more accurate model of the human condition, allowing a variety of genotypes and susceptibilities to be studied. However, unlike the monogenic models, there are no WT controls. By including a strain-matched control, TallyHo/JngJ that do not develop diabetes could potentially provide proper WT controls.

There are several limitations to our study: the first being that TallyHo/JngJ mice developing T2DM do not show significant changes in the bone phenotype, further raising the question if it can be used as a model for diabetic bone disease. In addition, sex-specific differences are observed in TallyHo/JngJ mice, as male mice tend to develop overt diabetes, which is characterized by hyperglycemia, insulin resistance, and other metabolic abnormalities. In contrast, the TallyHO/JngJ females tend to have moderate hyperinsulinemia, hyperlipidemia, and obesity without developing overt diabetes, such as hyperglycemia. A general limitation of animal models of diabetic bone disease is that both monogenic and polygenic models of T2DM show low BMD; this is counter-intuitive since patients with T2DM show normal to slightly increased BMD.

Although the full length of mature miRNAs (∼22 nt) is preserved within otherwise degraded RNA, we observed that those cortical bone RNA samples that showed lower RIN required a higher PCR amplification to generate enough DNA library compared to bone marrow total RNA samples. We hypothesize that the stronger presence of other short RNA fragments in degraded total RNA reduced the efficiency

of miRNA ligation and amplification during the library preparation. Ultimately, this may lead to reduced diversity and under-representation of certain miRNA sequences due to PCR bias. Therefore, the same no. of PCR cycles was applied to all cortical bone samples, reducing bias within this sample type. The quality of cortical bone NGS data for miRNAs is evidenced by the high no. of detected miRNAs as well as the homogenous and distinct clustering of all cortical bone RNA samples (see heatmap in Figure S2).

The prediction and analysis of miRNA targets is limited by high false-positive and false-negative rates of miRNA target prediction algorithms. Therefore, our target analyses have only considered experimentally verified interactions using the databases miRTarBase v8.0 and TarBase v8.0 for gene target analysis. However, 2 limitations remain with this approach: first, the experimental verifications reported in public databases are likely incomplete, which means that our analysis likely missed several confirmed target genes. Second, experimental verifications are performed with varying rigor, which means that our list of target genes may still include false positive interactions. Ultimately, to verify the mechanisms of miRNA contribution to diabetic bone disease, further *in-vitro* and *in-vivo* studies are required.

Our study provides a comprehensive NGS dataset describing the dysregulation of miRNAs in bone marrow, cortical bone tissue, and serum samples collected from a polygenic model of T2DM. We successfully confirmed the robustness of the NGS dataset by performing RT-qPCR analysis for a selected panel of miRNAs in the same samples. However, no validation in an independent animal cohort could be performed to demonstrate the biological reproducibility of our results.

In summary, the main limitations of this study concern the additional experimental validation of miRNA–mRNA target validation, the suitability of the TallyHo/JngJ model for diabetic bone disease research, and the availability of additional animal cohorts and samples to conduct an independent validation. These limitations are fully recognized and outlined in our manuscript. Nevertheless, we believe that the strengths of our study, including the comprehensive NGS analysis, qPCR validation, consistency with previous research, and rigorous bioinformatics analyses, provide a solid basis for our conclusions.

Conclusions

1. Since diabetic TallyHo/JngJ has the same bone phenotype as non-diabetic TallyHo/JngJ, we can affirm that the different bone phenotype in diabetic TallyHo/JngJ compared to SWR is not entirely due to diabetes but probably due to the different genetic background. Thus, epigenetics could play a role and induce the worse bone quality found in diabetic TallyHo/JngJ compared to SWR mice.
2. This is further evidenced by the fact that there is no dysregulation in cortical bone of TallyHo/JngJ mice compared to non-diabetic TallyHo/JngJ and by the high miRNA dysregulation in bone and bone marrow of TallyHo/JngJ mice compared to the SWR control.
3. The miRNA dysregulation in bone marrow of TallyHo/JngJ mice compared to SWR is reflected as well in the circulation, making these miRNA potential candidates as circulating biomarkers for low bone quality in TallyHo/JngJ mice. This is also supported by their roles in bone physiology, as shown by network analysis.

Acknowledgments

Small RNA-Seq was performed by the Next Generation Sequencing Facility at Vienna BioCenter Core Facilities (VBCF), a member of the Vienna BioCenter (VBC), Austria. Marianne Pultar, employed at TAmiRNA GmbH, gave excellent technical support related to the bioinformatic data analysis and uploading of the data in the Gene Expression Omnibus repository. Kseniya Khamina, employed at TAmiRNA GmbH, gave excellent support related to the library preparation for small RNA-Seq. Sarah Moussa and Teresa L. Krammer, both employed at TAmiRNA GmbH, gave excellent support related to the laboratory work.

Author contributions

David Carro Vázquez (Conceptualization, Data curation, Formal analysis, Methodology, Visualization, Writing—original draft, Writing—review & editing), Lejla Emini (Conceptualization, Formal analysis, Methodology, Writing—original draft, Writing—review & editing), Martina Rauner (Conceptualization, Funding acquisition, Methodology, Supervision, Writing—review & editing), Christine Hofbauer (Resources), Susanna Skalicky (Validation), Alisia Wagner (Validation), Johannes Grillari (Supervision, Writing—review & editing), Andreas B. Diendorfer (Formal analysis, Software), Lorenz C. Hofbauer (Funding acquisition, Methodology, Writing—review & editing), and Matthias Hackl (Conceptualization, Formal analysis, Funding acquisition, Methodology, Supervision, Writing—review & editing)

David Carro Vázquez and Lejla Emini contributed equally to this article.

Supplementary material

Supplementary material is available at *JBMR Plus* online.

Funding

This project has received funding from the European Union's Horizon 2020 Research and Innovation Programme under the Marie Skłodowska-Curie grant agreement No. 860898.

Conflicts of interest

During the performance of this research project, D.C.V. was employed at TAmiRNA GmbH.

A.B.D. is employed at TAmiRNA GmbH. M.H. is CEO and cofounder of TAmiRNA GmbH. J.G. is cofounder and scientific advisor of TAmiRNA GmbH.

Data availability

The sequencing data are available in the Gene Expression Omnibus repository (GSE201231).

References

1. Atkinson MA, Eisenbarth GS, Michels AW. Type 1 diabetes. *Lancet*. 2014;383(9911):69–82. https://doi.org/10.1016/S0140-6736(13)60591-7
2. Chatterjee S, Khunti K, Davies MJ. Type 2 diabetes. *Lancet*. 2017;389(10085):2239–2251. https://doi.org/10.1016/S0140-6736(17)30058-2

3. "World Health Organization." Accessed May 16, 2023. [Online]. https://www.who.int/health-topics/diabetes#tab=tab_1
4. Hofbauer LC, Busse B, Eastell R, et al. Bone fragility in diabetes: novel concepts and clinical implications. *Lancet Diabetes Endocrinol*. 2022;10(3):207–220. https://doi.org/10.1016/S2213-8587(21)00347-8
5. Napoli N, Chandran M, Pierroz DD, Abrahamsen B, Schwartz AV, Ferrari SL. Mechanisms of diabetes mellitus-induced bone fragility. *Nat Rev Endocrinol*. 2016;13(4):208–219. https://doi.org/10.1038/nrendo.2016.153
6. Kvist AV, Nasser MI, Vestergaard P, Frost M, Burden AM. Site-specific fracture incidence rates among patients with type 1 diabetes, type 2 diabetes, or without diabetes in Denmark (1997–2017). *Diabetes Care*. 2023;46(3):633–642. https://doi.org/10.2337/DC22-1004
7. Picke AK, Campbell G, Napoli N, Hofbauer LC, Rauner M. Update on the impact of type 2 diabetes mellitus on bone metabolism and material properties. *Endocr Connect*. 2019;8(3):R55–R70. https://doi.org/10.1530/EC-18-0456
8. Hammes HP, Alt A, Niwa T, et al. Differential accumulation of advanced glycation end products in the course of diabetic retinopathy. *Diabetologia*. 1999;42(6):728–736. https://doi.org/10.1007/S001250051221
9. Chen X, Ayala I, Shannon C, et al. The diabetes gene and Wnt pathway effector TCF7L2 regulates adipocyte development and function. *Diabetes*. 2018;67(4):554–568. https://doi.org/10.2337/db17-0318
10. Baron R, Gori F. Targeting WNT signaling in the treatment of osteoporosis. *Curr Opin Pharmacol*. 2018;40:134–141. https://doi.org/10.1016/J.COPH.2018.04.011
11. Zhou YT, Grayburn P, Karim A, et al. Lipotoxic heart disease in obese rats: implications for human obesity. *Proc Natl Acad Sci USA*. 2000;97(4):1784–1789. https://doi.org/10.1073/PNAS.97.4.1784
12. Du X, Edelstein D, Obici S, Higham N, Zou MH, Brownlee M. Insulin resistance reduces arterial prostacyclin synthase and eNOS activities by increasing endothelial fatty acid oxidation. *J Clin Invest*. 2006;116(4):1071–1080. https://doi.org/10.1172/JCI23354
13. Leanza G, Cannata F, Faraj M, et al. Bone canonical Wnt signaling is downregulated in type 2 diabetes and associates with higher advanced glycation end-products (AGEs) content and reduced bone strength. *Elife*. 2024;12:RP90437. https://doi.org/10.1101/2023.10.06.23296647
14. Piccoli A et al. Sclerostin regulation, microarchitecture, and advanced glycation end-products in the bone of elderly women with type 2 diabetes. *J Bone Miner Res*. 2020;35(12):2415–2422. https://doi.org/10.1002/JBMR.4153
15. Leanza G, Cannata F, Faraj M, et al. Wnt signaling regulation in bone of postmenopausal women with type 2 diabetes. *eLife*. 2023;12:RP90437. https://doi.org/10.7554/ELIFE.90437
16. Heilmeier U, Hackl M, Skalicky S, et al. Serum miRNA signatures are indicative of skeletal fractures in postmenopausal women with and without type 2 diabetes and influence osteogenic and adipogenic differentiation of adipose tissue–derived mesenchymal stem cells in vitro. *J Bone Miner Res*. 2016;31(12):2173–2192. https://doi.org/10.1002/jbmr.2897
17. Weilner S, Skalicky S, Salzer B, et al. Differentially circulating miRNAs after recent osteoporotic fractures can influence osteogenic differentiation. *Bone*. 2015;79:43–51. https://doi.org/10.1016/J.BONE.2015.05.027
18. Hackl M, Heilmeier U, Weilner S, Grillari J. Circulating microRNAs as novel biomarkers for bone diseases—complex signatures for multifactorial diseases? *Mol Cell Endocrinol*. 2016;432:83–95. https://doi.org/10.1016/J.MCE.2015.10.015
19. Lu TX, Rothenberg ME. MicroRNA. *J Allergy Clin Immunol*. 2018;141(4):1202–1207. https://doi.org/10.1016/J.JACI.2017.08.034
20. Carro Vázquez D, Emini L, Rauner M, et al. Effect of anti-osteoporotic treatments on circulating and bone microRNA patterns in osteopenic ZDF rats. *Int J Mol Sci*. 2022;23(12):6534. https://doi.org/10.3390/IJMS23126534
21. Liang YZ, Li JJH, Xiao HB, He Y, Zhang L, Yan YX. Identification of stress-related microRNA biomarkers in type 2 diabetes mellitus: a systematic review and meta-analysis. *J Diabetes*. 2020;12(9):633–644. https://doi.org/10.1111/1753-0407.12643
22. Zhu H, Leung SW. Identification of microRNA biomarkers in type 2 diabetes: a meta-analysis of controlled profiling studies. *Diabetologia*. 2015;58(5):900–911. https://doi.org/10.1007/S00125-015-3510-2
23. Kim JH, Kim JH, Stewart TP, et al. Phenotypic characterization of polygenic type 2 diabetes in TALLYHO/JngJ mice. *J Endocrinol*. 2006;191(2):437–446. https://doi.org/10.1677/joe.1.06647
24. Kim JH, Stewart TP, Zhang W, Kim HY, Nishina PM, Naggert JK. Type 2 diabetes mouse model TallyHo carries an obesity gene on chromosome 6 that exaggerates dietary obesity. *Physiol Genomics*. 2005;22:171–181. https://doi.org/10.1152/physiolgenomics.00197.2004
25. Kim JH, Saxton AM. The TALLYHO mouse as a model of human type 2 diabetes. *Methods Mol Biol*. 2012;933:75–87. https://doi.org/10.1007/978-1-62703-068-7_6
26. Emini L, Salbach-Hirsch J, Krug J, et al. Utility and limitations of TALLYHO/JngJ as a model for type 2 diabetes-induced bone disease. *JBMR Plus*. 2023;7(12):e10843. https://doi.org/10.1002/JBM4.10843
27. Kocijan R, Weigl M, Skalicky S, et al. MicroRNA levels in bone and blood change during bisphosphonate and teriparatide therapy in an animal model of postmenopausal osteoporosis. *Bone*. 2020;131:115104. https://doi.org/10.1016/j.bone.2019.115104
28. Khamina K, Diendorfer AB, Skalicky S, et al. A MicroRNA Next-Generation-Sequencing Discovery Assay (miND) for Genome-Scale Analysis and Absolute Quantitation of Circulating MicroRNA Biomarkers. *Int J Mol Sci*. 2022;23(3):1226. https://doi.org/10.3390/ijms23031226
29. Diendorfer A, Khamina K, Pultar M, Hackl M. miND (miRNA NGS Discovery pipeline): a small RNA-seq analysis pipeline and report generator for microRNA biomarker discovery studies. *F1000Research*. 2022;11:233. https://doi.org/10.12688/f1000research.94159.1
30. de Rie D, Abugessaisa I, Alam T, et al. An integrated expression atlas of miRNAs and their promoters in human and mouse. *Nat Biotechnol*. 2017;35:872–878. https://doi.org/10.1038/nbt.3947
31. Devlin MJ, van Vliet M, Motyl K, et al. Early-onset type 2 diabetes impairs skeletal acquisition in the male TALLYHO/JngJ mouse. *Endocrinology*. 2014;155(10):3806–3816. https://doi.org/10.1210/EN.2014-1041
32. Kujawa M. MicroRNA-466 and microRNA-200 increase endothelial permeability in hyperglycemia by targeting Claudin-5. *Mol Ther Nucleic Acids*. 2022;29:259–271. https://doi.org/10.1016/J.OMTN.2022.07.002
33. Sun Y, Zhou J, Shi L, Li J, Chen J. MicroRNA-466 inhibits cell proliferation and invasion in osteosarcoma by directly targeting insulin receptor substrate 1. *Mol Med Rep*. 2019;19(4):3345–3352. https://doi.org/10.3892/MMR.2019.9956
34. Kovacs P, Hanson RL, Lee YH, et al. The role of insulin receptor substrate-1 gene (IRS1) in type 2 diabetes in Pima Indians. *Diabetes*. 2003;52(12):3005–3009. https://doi.org/10.2337/DIABETES.52.12.3005
35. Wang JM, Qiu Y, Yang ZQ, Li L, Zhang K. Inositol-requiring enzyme 1 facilitates diabetic wound healing through modulating microRNAs. *Diabetes*. 2017;66(1):177–192. https://doi.org/10.2337/DB16-0052
36. Tagne JB et al. Transcription factor and microRNA interactions in lung cells: an inhibitory link between NK2 homeobox 1, miR-200c and the developmental and oncogenic factors Nfib and Myb. *Respir Res*. 2015;16(1):22. https://doi.org/10.1186/S12931-015-0186-6

37. Hou Q, Huang Y, Luo Y, et al. MiR-351 negatively regulates osteoblast differentiation of MSCs induced by (+)-cholesten-3-one through targeting VDR. *Am J Transl Res*. 2017;9(11):4963.
38. Song Y, Wu L, Li M, et al. Down-regulation of MicroRNA-592 in obesity contributes to hyperglycemia and insulin resistance. *EBioMedicine*. 2019;42:494–503. https://doi.org/10.1016/J.EBIOM.2019.03.041
39. Boucherat O, Agrawal V, Lawrie A, Bonnet S. Mitochondrial HSP90 accumulation promotes vascular remodeling in pulmonary arterial hypertension. *Am J Respir Crit Care Med*. 2018;198(1):90–103. https://doi.org/10.1164/RCCM.201708-1751OC
40. Yan C, Shi Y, Yuan L, et al. Mitochondrial quality control and its role in osteoporosis. *Front Endocrinol (Lausanne)*. 2023;14:149. https://doi.org/10.3389/FENDO.2023.1077058/BIBTEX
41. Panda AC et al. miR-196b-mediated translation regulation of mouse Insulin2 via the 5′UTR. *PLoS One*. 2014;9(7):101084. https://doi.org/10.1371/JOURNAL.PONE.0101084
42. Liu S, Liu D, Chen C, et al. MSC transplantation improves osteopenia via epigenetic regulation of notch signaling in lupus. *Cell Metab*. 2015;22(4):606–618. https://doi.org/10.1016/J.CMET.2015.08.018
43. Pethő A, Chen Y, George A. Exosomes in extracellular matrix bone biology. *Curr Osteoporos Rep*. 2018;16(1):58–64. https://doi.org/10.1007/S11914-018-0419-Y

JBMR Plus, 2025, 9, ziae121
https://doi.org/10.1093/jbmrpl/ziae121
Research Article